



Continuum percolation of two-dimensional adaptive dynamics systems

Chang Liu, Jia-Qi Dong ,* Lian-Chun Yu, and Liang Huang

Lanzhou Center for Theoretical Physics, Key Laboratory of Quantum Theory and Applications of MoE and Key Laboratory of Theoretical Physics of Gansu Province, Lanzhou University, Lanzhou, Gansu 730000, China

 (Received 28 August 2023; revised 21 May 2024; accepted 17 July 2024; published 5 August 2024)

The percolation phase transition of a continuum adaptive neuron system with homeostasis is investigated. In order to maintain their average activity at a particular level, each neuron (represented by a disk) varies its connection radius until the sum of overlapping areas with neighboring neurons (representing the overall connection strength in the network) has reached a fixed target area for each neuron. Tuning the two key parameters in the model, i.e., the density defined as the number of neurons (disks) per unit area and the sum of the overlapping area of each disk with its adjacent disks, can drive the system into the critical percolating state. These two parameters are inversely proportional to each other at the critical state, and the critical filling factors are fixed about 0.7157, which is much less than the case of the continuum percolation with uniform disks. It is also confirmed that the critical exponents in this model are the same as the two-dimensional standard lattice percolation. Although the critical state is relatively more sensitive and exhibits long-range spatial correlation, local fluctuations do not propagate in a long-range manner through the system by the adaptive dynamics, which renders the system overall robust against perturbations.

DOI: [10.1103/PhysRevE.110.024111](https://doi.org/10.1103/PhysRevE.110.024111)

I. INTRODUCTION

Percolation is probably the simplest model exhibiting phase transition in physics [1–3]. It was first presented to describe the connectivity property of the fluid flow in porous media [4]. In general, percolation models can be grouped into different universality classes, defined by a set of critical exponents characterizing the scaling behavior of collective quantities [5–8]. One typical example is the site percolation on two-dimensional (2D) square lattices. Each site on the lattice is occupied with probability p . Neighboring occupied sites are considered to be connected and form clusters. With the occupying probability p surpassing the percolation threshold p_c , the clusters merge into a spanning cluster, either reaching the opposite sides of the infinite lattice or containing a nonzero fraction of the sites in the thermodynamic limit. Besides the discrete percolation model, there is a large class of percolation phenomena in the continuum medium, where the number of objects is countable, but the position and the connecting radius are in the continuous space, including conducting materials [9–12], elastic behavior of composites [13–15], *ad hoc* networks [16,17], connectivity in cultured neuronal networks [18,19], and so on. These investigations usually consider that the objects are placed randomly in the system [20], which takes regular shapes, such as squares [21], disks [22], or sticks [23,24], and can overlap randomly with neighboring objects with a uniform or a particular angular distribution [24] or size distribution [25]. The emergence of the spanning cluster is crucial to these systems, such as conductivity for fluid flow or electronic currents, and connectivity for supporting global site-to-site communications. Typically, the discrete and

continuum percolation models with the same spatial dimension share the same critical exponents and thus belong to the same universal class [26–28].

Adaptive dynamics are ubiquitous in natural and engineered systems consisting of evolving and interacting components, such as game theory [29,30], financial markets [31], power grid systems [32], engineered multilayer systems with the target of enhancing the robustness [33], growing neural systems [34,35], and so on. Particularly, the formation of connectivity during the development of the nervous system connects disjoint components into a spanning cluster, which is the basis for the proper functioning of the neural system. Abstracting from any details, we imagine that in quasi-two-dimensional culturing systems, each neuron can be represented by a disk, whose center corresponds to the neuron's location and whose radius determines the range over which it can generate synapse connections with neighboring neurons. Therefore, if the disks of two neighboring neurons are overlapped, they are able to establish synapse connections. It is assumed that the synaptic coupling strength is proportional to the overlapping areas. In general, neurons exhibit homeostasis and maintain their average activity at a particular level, i.e., those with low activity level extend their neurites and form more activating connections, while highly active cells reduce their connections [36]. For simplicity, it is assumed that the target overlapping area is the same for all. In this way, the system will evolve into an equilibrium critical state with connected neuron clusters. This is similar to the continuum percolation model, but with features that have not been considered before.

In this work, we propose a model of continuum percolation on a two-dimensional plane to take into account the adaptive dynamical features of homeostasis in neuronal systems, where each disk (neuron) adaptively expands or shrinks in time to

*Contact author: dongjq@lzu.edu.cn

approach a prescribed target overlapping area with its neighboring disks. When for all the disks the target overlapping area is reached, the dynamical evolution stops, and clusters of connected (overlapped) disks are counted for percolation analysis.

In addition to the aforementioned percolation models, there is a “touch-and-stop” cluster growth percolation model (CGP) [37–39], which belongs to the standard percolation universality class [39]. In this model, a number of active seeds placed on random locations are growing in all directions at a constant rate to form clusters. Once a cluster is in contact with another, its growth stops immediately. Intuitively, this model could be a particular case for our model in the discrete lattices when the overlapping area is set to 0. However, as we show later, this is not the case.

Instead of only one control parameter for typical percolation models, for our model, there are two parameters: one is the target overlapping area Δ for each disk, and the other is the density ρ of the disks in the domain. Therefore, in the (ρ, Δ) parameter plane, there will be a line separating the subcritical and supercritical phases. A critical curve has been noticed before in different variants of the standard percolation model, e.g., the sol-to-gel transition (gelation) of polymers [40], the dissociative adsorption of dimers [41], and mixed site-bond percolation models [42–45]. However, for our model, the effect of varying Δ is more like an implicit spatial scale scaling in mathematics, which will be discussed in the following section. It may be a succinct way to select any one of the two parameters as the control parameter, while the other is designated as the system parameter, though these two parameters have separate physical meanings. In this paper, the relation between ρ and Δ is determined numerically at a critical point, and the critical exponents are also obtained, which demonstrates the model belongs to the same universal class as the other 2D percolation models. And an intriguing phenomenon that may contradict common sense is that the local fluctuation of the overlapping area does not propagate in a long-range manner through the system by the adaptive dynamics, even at percolation thresholds. This may be the reason why the dynamics does not encounter frustration.

The rest of this paper is organized as follows. In Sec. II, we discuss the adaptive dynamical model in detail. In Sec. III, we present the main results of the critical behavior of the model, and the propagation properties of the local fluctuation of the model around critical state. Conclusions are summarized in Sec. IV.

II. MODEL

The two-dimensional continuum percolation model governed by adaptive dynamics is as follows (see Fig. 1). The system consists of N disks randomly scattered in a square of length L . Initially, the radius of a disk is set to the shortest distance to its neighboring disks. Thus the disks at the initial state have overlapped areas. This setup speeds up the convergence of the dynamics, but is irrelevant to the percolation results. The radius r_i of disk i evolves in two steps. First, r_i is incremented by

$$r_i(n) = r_i(n-1) + Kr_i(n-1), \quad (1)$$

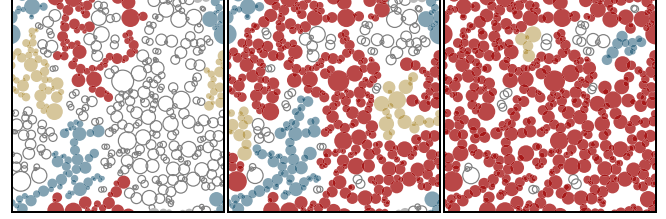


FIG. 1. The largest three clusters of the adaptive dynamical system with periodic boundary conditions for three snapshots at the steady state. The red (dark gray), blue (medium gray), and yellow (light gray) correspond to the clusters with size decreasing. The empty circles represent other disks. From left to right, the target overlapping area $\Delta = 0.0445, 0.0945,$ and $0.1345,$ respectively. The density is $\rho = 2$ and the side length of the system is $L = 16,$ the corresponding percolation threshold is $\Delta_c \simeq 0.0945.$ The center of the disks for different cases have the same location configuration.

where n is the discrete time. K controls the growth rate of all the disks of the system and is set to $K = 0.01$ in our simulation. Then, the radius evolution equation for the second step is decided based on the overlapping area. If the disk i has no overlapping area with any disk, the radius r_i evolves one more step based on Eq. (1). Otherwise, r_i changes as follows,

$$r_i(n+1) = r_i(n-1) + \frac{\Delta - \sum_j A_{ij}(n-1)}{\sum_j [A_{ij}(n) - A_{ij}(n-1)]} Kr_i(n-1), \quad (2)$$

where $A_{ij}(n)$ is the overlapping areas between disk i and disk j at the n th step. The radius of each disk is evolved to achieve the objective of the adaptive dynamics, i.e., the target overlapping area Δ . If each disk i satisfies $\sum_j A_{ij} = \Delta$, the system stops evolving and reaches a steady state. The extreme situations of unrestricted growth or constriction are avoided within the constraints of the adaptive dynamics. A detailed explanation of the Eq. (2) is presented in the Appendix A.

In this model, there are two control parameters, one is the density $\rho = N/L^2$, defined as the ratio of the number of the randomly scattered disks N to the area of the square system of length L . The other control parameter is the target overlapping area Δ , which describes the adaptive dynamics and determines whether the radius of disks will grow or contract. It also determines the degree of the overlapping of the disks and thus the connectivity of the neurons. Therefore, in the infinite size limit, the percolation threshold depends on both of these two parameters (ρ, Δ) , whereas in most previous studies the percolation threshold in general only depends on the density ρ [1,20].

For an infinite system, the critical state does not change due to the scaling of the spatial scale. Supposing that space shrinks by a factor α , the density of disks and the overlapping areas are rescaled as $\rho \rightarrow \rho/\alpha^2$ and $A_{ij} \rightarrow A_{ij}\alpha^2$. Since the target Δ is the linear summation of overlapping area A_{ij} , it can be conjectured that the critical states with different parameters can be regarded as an effect of space extending (or shrinking) described by Δ . Therefore, the curve consisting of diverse sets of critical points should follow a simple relation, i.e., $\rho_c \sim \Delta^{-1}$, and then the critical state of the system on any point of the critical curve should be identical. It should be

noted that this discussion appears to be a consequence of the linear summation of the overlapping area to reach the target value Δ in the adaptive dynamics. For more complicated target functions, the aforementioned relation might be broken.

III. RESULTS

A. Percolation properties

For continuous phase transition, the order parameters exhibit power-law behavior at the phase transition point, where the critical exponents are represented by the power exponents. According to whether their values are the same, the critical exponents are used to identify if the phase transitions on different systems belong to the same universality class. In this section, we calculate the critical exponents of this model and find that it belongs to the same universality class as the conventional two-dimensional discrete percolation.

Compared to the conventional continuum percolation, the introduction of adaptive dynamics additionally introduces a new control parameter Δ . These two control parameters can be varied independently to achieve a critical state, and the finite-size effects of varying the two parameters to approach a critical state are similar. In the subsequent part of this section, we focus on the control parameter density ρ , and the target overlapping area Δ , as the system parameter, is set to be 0.2. Additional numerical results of varying Δ as control parameter are detailed in Appendix B.

Near the critical point, if the percolation phase transition is continuous, the largest cluster S_1 consisting of overlapping disks in percolation should satisfy the finite-size scaling in the form of [46]

$$S_1(\rho, L; \Delta) = L^{d_f} F_{1,\rho}(t_\rho L^{1/\nu}; \Delta), \quad (3)$$

where d_f is the fractal dimension of the cluster, which should be the same for the largest and the second largest cluster, F_1 is the scaling function of the largest cluster. L is the system length, and $t_\rho = (\rho - \rho_c)/\rho_c$ represents the deviation of the density from the critical point ρ_c . Due to the hyperscaling relation for the equilibrium system, there are only two independent critical exponents [26]. Here we choose the fractal dimension of the cluster d_f and the critical exponent ν of the correlation length $\xi \sim |t_\rho|^{-\nu}$ in our study.

Likewise, the second largest cluster S_2 can also be expressed in a finite-size scaling form around the critical point

$$S_2(\rho, L; \Delta) = L^{d_f} F_{2,\rho}(t_\rho L^{1/\nu}; \Delta), \quad (4)$$

where F_2 is the scaling function for the second largest cluster.

Then the finite-size scaling form of the ratio can be obtained by using Eqs. (3) and (4):

$$\frac{S_1}{S_2} \equiv U_\rho(t_\rho L^{1/\nu}; \Delta). \quad (5)$$

At the critical point of the density, $t_\rho = 0$,

$$\left. \frac{S_1}{S_2} \right|_{t_\rho=0} = U_\rho(0; \Delta), \quad (6)$$

indicating that the ratio is independent of the system size L . As a side note, the largest cluster size $S_1(L)$ has high-order

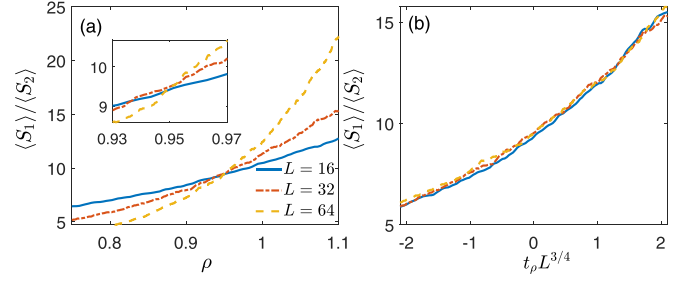


FIG. 2. (a) The ratio of the size of the largest cluster and that of the second largest cluster $\langle S_1 \rangle / \langle S_2 \rangle$ for systems with different sizes. The inset shows the zoom-in plots around the critical points, which are $\rho_c \simeq 0.951$. (b) Rescale the horizontal coordinate using t_ρ and make the curves coincide by adjusting $\nu = 4/3$. Each data point is an average of 10^3 ensembles.

correction at the critical point, $S_1(L) = L^{d_f} F_{1,\rho}(0, L)(1 + cL^{-x})$, where c and x are constants [47]. The correction cL^{-x} usually results in an imperfect intersection, as shown in the insets of Fig. 2. In estimation, the relative deviation $(\rho'_c - \rho_c)/\rho_c$ of critical point caused by the correction approaches to $L^{-1/\nu-x}$, and in this model, the relative deviation can be less than 0.002, which is demonstrated subsequently. Thus, the high-order correction of S_1 can be disregarded in estimating critical points. Consequently, the curves of S_1/S_2 cross at the same point at ρ_c for different system sizes with the same Δ . This feature can be used to determine the critical point of the model.

Figure 2(a) shows the ratio of the mean largest cluster to the mean second largest cluster $\langle S_1 \rangle / \langle S_2 \rangle$ as a function of ρ . The curves of $\langle S_1 \rangle / \langle S_2 \rangle$ for different sizes L cross at a single point in the $(\rho, \langle S_1 \rangle / \langle S_2 \rangle)$ plane, which is $\rho_c \approx 0.951$ for $\Delta = 0.2$. According to Eq. (6), the curves of $\langle S_1 \rangle / \langle S_2 \rangle$ vs $L^{1/\nu} t_\rho$ should be L independent, and the curves for different size L will be overlapped on top of each other. Thus the value of ν can be determined by tuning ν to make the curves coincident. Figure 2(b) plots the curves of $\langle S_1 \rangle / \langle S_2 \rangle$ vs $L^{1/\nu} t_\rho$ with $\nu = 4/3$. The curves overlap each other roughly, thus the obtained critical exponent of the correlation length is about $\nu = 4/3$, which is the same as the critical exponent ν in lattice percolation.

The critical exponent ν can also be estimated more accurately from the position of the peak in $S_2(L)$. Similar to site percolation, a peak appears in the size of the second largest cluster near the critical point. According to the finite-size scaling Eq. (4), the reduced control parameter t_ρ^{peak} of the peak position has a scaling form, $t_\rho^{\text{peak}} \propto L^{-1/\nu}$. The inverse critical exponents $-1/\nu$, that is the slope of the dashed line in Fig. 3(a), is -0.7487 for controlling ρ . This value is consistent with the theoretical exponent ν in the 2D percolation universality class.

In general, for an equilibrium system, there are two independent critical exponents to characterize the critical properties, while all the others can be calculated by hyperscaling relations [6]. Here besides ν , we perform simulations at ρ_c to determine the fractal dimension d_f , which is defined by $\langle S \rangle \propto L^{d_f}$. Figure 3(b) shows the size of the largest cluster $\langle S_1 \rangle$ and the second largest cluster $\langle S_2 \rangle$ at ρ_c for different

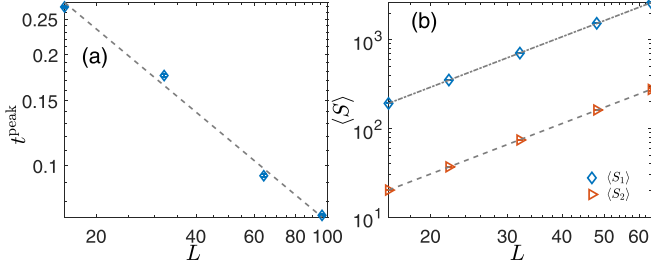


FIG. 3. (a) Reduced position of $S_2(L)$ peak varying with system size. (b) The average size of the largest cluster $\langle S_1 \rangle$ (diamonds) and the second largest cluster $\langle S_2 \rangle$ (triangles) at the critical point as a function of the system size L . The slope of the fitting lines corresponds to the fractal dimension d_f , which is about 1.886(8). Each symbol is an average of 10^4 different realizations.

system sizes, the curves are fitted according to the scaling form $\langle S \rangle(L) = aL^{d_f}$, where a is a fitting coefficient, and $d_f \simeq 1.886(8)$ for all cases, which is approximately the same as the fractal dimension $d_f = 91/48 \approx 1.8958$ for 2D lattice percolation. The linearity of the $S_1(L)$ in the log-log coordinate can measure the accuracy of the critical point. With ρ deviating ρ_c , the linearity of the logarithmic order parameter $\log[S_1(L)/N]$ decreases, and as shown in Fig. 4(a), the accuracy of the critical point estimated by the intersection of S_1/S_2 is about 0.002. The critical exponents β and γ can be estimated from the order parameter at the critical, since the following scaling relation

$$\begin{aligned} S_1(\rho_c, L; \Delta)/N &\propto L^{\beta/\nu} \\ \chi(\rho_c, L; \Delta) &\propto L^{\gamma/\nu}, \end{aligned} \quad (7)$$

where χ is the fluctuation of the order parameter, i.e., $\chi = N[(\langle S_1/N \rangle)^2 - \langle S_1^2/N^2 \rangle]$ [39] shown in Fig. 4(b). Combined with the value of the exponent ν , the critical exponents are 0.144(8) and 2.42(5) corresponding β and γ , respectively, which are also consistent with the 2D percolation universality class. Based on these four obtained from the fitting data, it can be considered that this percolation model with adaptive dynamics belongs to the general universality class of the 2D

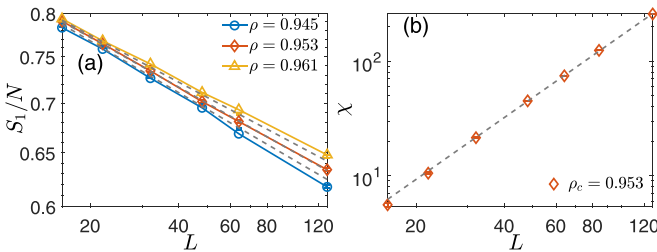


FIG. 4. (a) The logarithmic order parameter $\log[S_1(L)/N]$ as a function of the system size with different ρ . Each symbol corresponds to a different control parameter. At the critical point $\rho = 0.953$ while $\Delta = 0.2$, the slope corresponds to β/ν , which is -0.1083 . (b) The order parameter fluctuation χ at a critical point as a function of system size. Fitting the different systems L results in $\gamma/\nu = 1.815$, which is consistent with the result of $\gamma/\nu = 43/24$ for the 2D percolation model. Each symbol is an average of 10^4 different realizations.

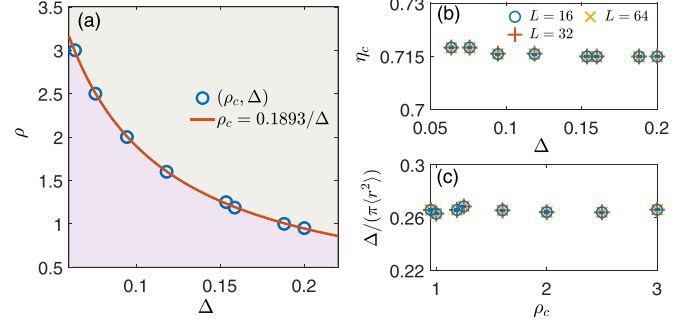


FIG. 5. The phase diagram. (a) Each blue circle represents a percolation threshold obtained by averaging over 10^4 different configurations for each of the three different system sizes. The fitting red curve of these percolation thresholds is $\rho_c = 0.1893/\Delta$, which divides the phase diagram into two regions, i.e., subcritical (below the line) and supercritical (above the line). (b) The filling factor η_c vs target overlapping area Δ . Despite the different parameter, the connectivity of the system η_c is almost the same at criticality, which is 0.7157(39). (c) The ratio between the target overlapping area Δ and the average area of disks $(\pi \langle r_i^2 \rangle)$ at the critical point. The ratio approaches a constant value, i.e., 0.2653(59). Each symbol in (b) and (c) is the result of averaging 10^4 realizations.

lattice percolation. Note that the critical point in our model depends on the value of the parameter Δ . We have determined several pairs of thresholds (ρ_c, Δ) in the parameter plane, and find that they can be fitted well by $\rho_c = 0.1893/\Delta$. The results are shown in Fig. 5(a). Below the curve, the clusters are all small and the system is subcritical; above the curve, there is a spanning cluster, and the system is in a percolated state. Our model can be related to a 2D continuum percolation model of randomly scattered N uniform disks with area A , where the existence of the percolation cluster depends only on the filling factor $\eta = NA/L^2$, under the condition that $L \rightarrow \infty$. For uniform disks, the critical filling factor is $\eta_c \approx 1.1281$ [20]. For our model, the area of disk i is πr_i^2 , a similar filling factor can be defined as,

$$\eta = \frac{\sum_{i=1}^N \pi r_i^2}{L^2} = \rho \pi \langle r_i^2 \rangle, \quad (8)$$

where $\pi \langle r_i^2 \rangle$ is the average area of all the disks. For different critical points (ρ_c, Δ) , we can calculate the corresponding η_c . It is found that although the critical points can be different, η_c takes almost a constant value of 0.7157(39) independent of Δ , as shown in Fig. 5(b), which suggests that the adaptive dynamics is more efficient to form the spanning clusters. The ratio of the overlapping area Δ to the mean area of disks is a fixed value at the critical point,

$$\frac{\Delta}{\pi \langle r_i^2 \rangle} \approx \text{const.}, \quad (9)$$

which is independent of ρ_c as shown in Fig. 5(c). The results in Fig. 5 provide the evidence of the conjecture mentioned in Sec. II that critical states with different Δ can be regarded as a consequence of shrinking or expanding space.

It should also be noted that the limiting case of $\Delta \rightarrow 0$ of our adaptive dynamics model will not reduce to the

TABLE I. Critical behavior, which characterizes the percolation phenomenon in two-dimensional systems with periodic boundary conditions. The site percolation model (SP), bond percolation model (BP), and the CGP model (disk-shaped clusters) are on the 2D square lattice, while the continuum percolation with disks (CPD) and our continuum percolation model with adaptive dynamics (CPA) are on the 2D continuum square region. p_c and η_c denote the threshold for discrete and continuum percolation, respectively. ν and d_f are two independent critical exponents, and take the same values. The critical exponents β and γ are also the same as for 2D SP. Therefore, although the critical thresholds are completely different, these models on discrete or continuum 2D media are in the same universality class.

	p_c	η_c	ν	d_f	β	γ
SP	0.592 746 21(13) [48]	—	4/3 [48]	91/48 [49]	5/36 [7]	43/18 [7]
BP	0.5 [50]	—	4/3 [51]	91/48 [52]	5/36 [7]	43/18 [7]
CGP	0.4978(5) [39]	—	1.32(4) [39]	1.8995(4) [39]	0.145(4) [39]	2.38(3) [39]
CPD	—	1.128 087 37(6) [20]	4/3 [20]	—	0.14(2) [26]	2.43(4) [26]
CPA	—	0.7157(39)	1.33(4)	1.886(8)	0.144(8)	2.42(5)

touch-and-stop continuum percolation model where the disks are not tangent to each other, as the ratio of the critical target overlapping area to the average area of the disks $\Delta_c/\pi \langle r^2 \rangle$ remains a constant, and the disks still have significant overlaps.

Table I lists the critical thresholds and critical exponents for the five different percolation models. Either discrete or continuous, they have the same critical exponents, giving a strong indication that these models are in the same universality class. The only difference is the value of the critical points p_c or η_c , which depends on the model details.

B. Properties of the system at different percolation phases

This model of continuous percolation originates from the adaptive neuron system considering the homeostasis effects. Since homeostatic plasticity adjusts the coupling strength of neurons to a specific level, fluctuations in the activity level of a single neuron can lead to adjustments in the coupling strength of distant neurons. This relevant dynamical issue is then at the steady state, if one neuron has a perturbation, how the perturbation propagates to the other neurons, and whether this property depends on the criticality of the percolating states. In this case, we fix the ρ and discuss the propagation of the fluctuation of the overlapping areas. Here, we fix $L = 16$ and consider three cases, i.e., $L^{1/\nu}(\Delta - \Delta_c)/\Delta_c = \pm a$, 0, where $a = 7$ is constant, for subcritical ($-a$), critical (0), and supercritical (a) when $\rho = 1$. Due to the interneuron correlation, a variation in the radius of a neuron not only affects its own size, but also causes variations of its adjacent neurons. This effect is not captured by other percolation models.

To be specific, a neuron or disk is randomly chosen when the system arrives at the steady state, and adds a small perturbation δ to its target overlapping area. Since the radius of the disks is not the same in the steady state, a perturbation applied on the radius causes a nonuniform relative magnitudes of the perturbations. To overcome this issue, the target overlapping area of the perturbed node i is increased or decreased not by an absolute value, but by a certain percentage, i.e., $\Delta_i \rightarrow (1 \pm \delta)\Delta$. After the system reaches the steady state again, the average changes in the disks' area, the size of the largest cluster, the number of clusters, and the size of the cluster containing the perturbed disk between the current state and the initial state are recorded. Since the system is composed of noncontact clusters, the perturbation typically only propagates within the cluster containing the initially perturbed disk.

In Fig. 6(a) the perturbed disk is selected in the largest cluster, and the propagation of the perturbation decays exponentially with the distance from the perturbed disk i at a critical point. Figure 6(b) demonstrates the absolute value of the largest-cluster-size difference of the systems before and after perturbation. In the three cases, the critical one is more sensitive to the changes in δ than the other cases, while the largest cluster size of the supercritical state is insensitive to the perturbation intensity. In the critical state, as the perturbation increases, the maximum difference does not exceed 1, that is, the largest cluster size in the system is not drastically changed after the perturbation due to adaptive dynamics. Similarly, in Fig. 6(c), the variation in the number of clusters n_c in the system increases with the perturbation intensity δ , but the variation $\langle |n_{c|_b} - n_c| \rangle$ is still less than 1. The amount of variation in the number of clusters depends on the state of the system. In subcritical, the system has a large number

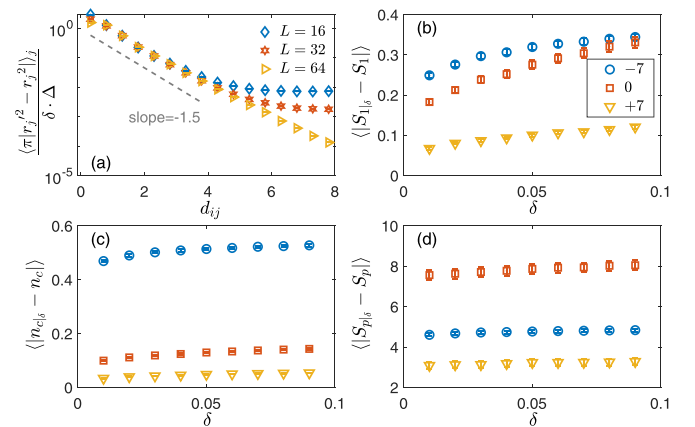


FIG. 6. (a) The average changes of the disks' area $\langle \pi |r_j^2 - r_j^2| \rangle_j$ vs the distance d_{ij} after the perturbation at the critical point. The perturbation intensity on the perturbed disk i is $\delta = 0.01$. Different symbols represent different system sizes. (b) Variation of the mean absolute value of the largest-cluster-size difference before and after the perturbation δ . (c) Similar to (b), the variation in the number of clusters is due to the perturbation. (d) Variation of the size of the cluster containing the perturbed disk, while the average size of the perturbed cluster remains almost constant. Circles, squares, and triangles represent the subcritical ($t_\Delta L^{1/\nu} = -7$), the critical ($t_\Delta = 0$), and the supercritical ($t_\Delta L^{1/\nu} = +7$) cases. The above results are the average of 100 configurations.

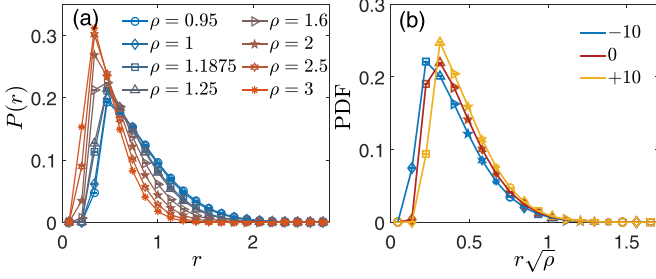


FIG. 7. (a) The radius distributions corresponding to different ρ at the critical state. (b) The rescaled radius $r\sqrt{\rho}$ distributions for $t_\rho L^{1/\nu} = \pm 10$ and 0. For each case, the lines with the same symbol are the results of eight densities ρ , which all collapse to each other. The distributions of the systems with different sizes and the same value of $t_\rho L^{1/\nu}$ are exactly identical. For simplicity, only the cases of $L = 64$ are shown here. 10^4 samples are taken for histogram.

of clusters with small sizes, so the variation in cluster number after the perturbation is the largest, while supercritical has a small number of clusters but a large size in the system, so the variation in cluster number is the smallest among the three states, and the variation in the critical state lies in between the two states.

Then considering the variation of the size S_p of the cluster containing the perturbed disk, shown in Fig. 6(d), it can be seen that the variation of the cluster with the perturbation $\langle |S_{p_i} - S_p| \rangle$ is more distinct than the variation of S_1 , especially at the critical state. For the clusters, to which the perturbed disk belongs, the perturbations can affect its size significantly. However, the effect of the perturbation can be absorbed by the surrounding disks quickly, i.e., the perturbation decays exponentially with increasing distance, as a result, the frustration or long-lasting oscillation of the disk area has not been observed in our simulation.

The radius distribution at the critical state, as shown in Fig. 7(a), is significantly different for different ρ . For small ρ , the radius distribution is broad and the peak is low, while as ρ gradually increases, the width of the distribution becomes narrower and the peak becomes higher. This is intuitively consistent with that smaller r_i to achieve the overlapping area is required for percolation at higher ρ . It should be emphasized that the radius distribution has no observable finite-size effect. The radius is mainly dominated by the distance of the adjacent disks, i.e., $1/\sqrt{\rho}$ on average. This effect for different ρ s can be included by the rescaling radius $r\sqrt{\rho}$. For fixed $t_\rho L^{1/\nu}$, the rescaled radius distributions are identical for systems with different L and ρ , as shown in Fig. 7(b).

IV. CONCLUSION AND DISCUSSIONS

Percolation on a continuum medium is a commonly observed phase transition phenomenon. Here we propose a continuum percolation model with adaptive dynamics based on a neuronal growth model with homeostatic plasticity. We have confirmed that this model belongs to the same universal class as the normal 2D percolation, by the correlation length critical exponent ν and the fractal dimension d_f . Besides the density ρ , in this model there is another control parameter, that is, the target overlapping area Δ due to the homeostatic

plasticity. However, for the linear summation of A_{ij} in the dynamics of homeostatic plasticity, a critical configuration of disks in infinite space can be deformed into a critical configuration of different densities by shrinking or expanding space, which corresponds to varying target overlapping area. Therefore, these two control parameters are inversely related at the critical point and can result in identical critical behavior. Based on the same reason, the critical filling factor is 0.7157, which is independent of the parameter target overlapping area.

Since the adaptive dynamics of the system is embodied with the growth or contraction of the radius for the disks, once there is a perturbation, it will propagate through the system. However, we find numerically that, although at the critical state, the system is relatively more sensitive in terms of the size of the largest cluster or the cluster containing the initially perturbed disk, the perturbation always decays exponentially with increasing distance, thus the system is stable against the perturbations, which could be a heritage of the neural dynamics with homeostasis.

Introducing adaptive dynamics into continuum percolation is an interesting point to enrich the universality class of percolation. From the perspective of investigations in complex systems, our work constitutes an interesting piece for understanding the structural evolution of adaptive systems, which are ubiquitous in natural and engineering systems, such as neural networks, *ad hoc* systems, and the collective motion of active matter systems.

ACKNOWLEDGMENTS

The authors sincerely thank the anonymous reviewers for their helpful comments and concrete suggestions. This work was supported by NSFC under Grants No. 12305045, No. 12175090, and No. 12247101, by the Fundamental Research Funds for the Central Universities under Grant No. Izujbky-2021-62, and by the 111 Project under Grant No. B20063.

APPENDIX A: RADIUS EVOLUTION EQUATION

The system can evolve to the target state only based on the dynamics of Eq. (1). To accelerate the rate of convergence, Eq. (2) is introduced. For the final state of the adaptive dynamics, i.e., $\mathbf{r}^* = [r_1^*, \dots, r_N^*]^T$, the total overlapping area $\sum_j A_{ij}(\mathbf{r}^*)$ of each disk is Δ . Around the state, the total overlapping area can be linearly approximated as

$$\mathbf{F}(\mathbf{r}^*) = \mathbf{F}(\mathbf{r}^* + \delta_1) - \left[\frac{\partial \mathbf{F}}{\partial \mathbf{r}} \Big|_{\mathbf{r}=\mathbf{r}^*+\delta_1} \right] \delta_1, \quad (\text{A1})$$

where $\mathbf{F}(\mathbf{r})$ is the function of total overlapping area defined as $\mathbf{F}(\mathbf{r}) \equiv [\sum_j A_{1j}(\mathbf{r}), \dots, \sum_j A_{Nj}(\mathbf{r})]^T$. After one-step evolution of Eq. (1), the total overlapping area function \mathbf{F} can be expanded as

$$\mathbf{F}(\mathbf{r}^* + \delta_2) = \mathbf{F}(\mathbf{r}^* + \delta_1) + \left[\frac{\partial \mathbf{F}}{\partial \mathbf{r}} \Big|_{\mathbf{r}=\mathbf{r}^*+\delta_1} \right] (\delta_2 - \delta_1), \quad (\text{A2})$$

where $\delta_2 - \delta_1$ is $K\mathbf{r}(n-1)$ and K is the constant in Eq. (1). Around the critical point, the topological structure of the disks' connection is sparse, and most elements of matrix $[\partial \mathbf{F} / \partial \mathbf{r}]$, except for the diagonal elements, are 0. Then, matrix $[\partial \mathbf{F} / \partial \mathbf{r}]$ is approximated as a diagonal matrix to reduce

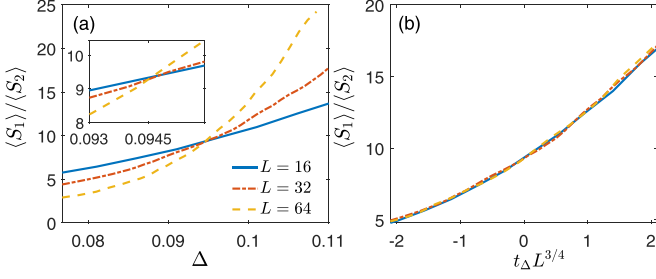


FIG. 8. (a) The ratio of the size of the largest cluster to the size of the second largest cluster $\langle S_1 \rangle / \langle S_2 \rangle$ for systems of different sizes when the control parameter is Δ , with $\rho = 2$. The inset shows the zoom-in plots around the critical point, which is ($\rho = 2$, $\Delta_c \simeq 0.0945$). (b) The same plot as (a) but with a rescaled horizontal axis by $t_\Delta L^{1/\nu}$. The curves of the data coincide by tuning ν to $4/3$. Thus this case has the same critical exponent of $\nu = 4/3$ with Fig. 2. Each data point is an average of 10^3 ensembles.

the amount of computation. Thus, combining Eq. (A1) and Eq. (A2), the matrix $[\partial F / \partial r]$ can be eliminated, i.e.,

$$\frac{F_i(\mathbf{r}^*) - F_i(\mathbf{r}^* + \delta_1)}{\delta_1(i)} = \frac{F_i(\mathbf{r}^* + \delta_2) - F_i(\mathbf{r}^* + \delta_1)}{\delta_1(i) - \delta_2(i)}, \quad (\text{A3})$$

and an iterative algorithm can be constructed as

$$r_i(n+1) = r_i(n-1) + \frac{F_i(\mathbf{r}^*) - F_i[\mathbf{r}(n-1)]}{F_i[\mathbf{r}(n)] - F_i[\mathbf{r}(n-1)]} K r_i(n-1), \quad (\text{A4})$$

where $F_i(\mathbf{r}^*) \equiv \Delta$ and $F_i \equiv \sum_j A_{ij}$. Essentially, this two-step process provides a measure of information of the matrix $[\partial F / \partial r]$ so that it can accelerate evolution. In this model, the convergence precision of the algorithm can be better than 10^{-8} , i.e., $\max[|F_1 - \Delta|, \dots, |F_N - \Delta|] < 10^{-8} \Delta$.

APPENDIX B: RESULTS FOR VARYING THE TARGET OVERLAPPING AREAS

Here are the results related to the critical phenomenon of varying the target overlapping area Δ . Near the critical point, the largest cluster and the second largest cluster should follow the finite-size scaling form similar to Eqs. (3) and (4) as following,

$$S_1(\Delta, L; \rho) = L^{d_f} F_{1,\Delta}(t_\Delta L^{1/\nu'}; \rho), \quad (\text{B1})$$

$$S_2(\Delta, L; \rho) = L^{d_f} F_{2,\Delta}(t_\Delta L^{1/\nu'}; \rho), \quad (\text{B2})$$

where $t_\Delta = (\Delta - \Delta_c) / \Delta_c$. Correspondingly, the ratio is given by

$$\frac{S_1}{S_2} \equiv U_\Delta(t_\Delta L^{1/\nu'}; \rho). \quad (\text{B3})$$

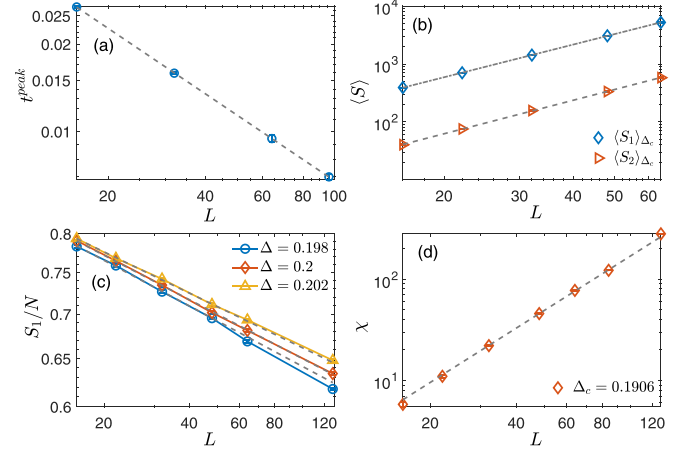


FIG. 9. The critical exponents are calculated when the system is in the percolation state, with the control parameter Δ . (a) Reduced position of $S_2(L)$ peak varying with system size when $\rho = 2$. (b) The average size of the largest cluster and the second largest cluster at the critical point as a function of the system size L . The slope of fitting lines corresponds to $d_f = 1.886(8)$. (c) The logarithmic order parameter $\log[S_1(L)/N]$ as a function of the system size with different Δ . At the critical point ($\Delta_c = 0.2$, $\rho = 0.953$), the slope corresponds to β/ν , which equals -0.1083 . (d) The order parameter fluctuation χ at critical point ($\Delta_c = 0.1906$, $\rho = 1$) as a function of system size, fitting the different systems L results in $\gamma/\nu = 1.815$. Each symbol is an average of 10^4 different realizations.

At the critical point, $t_\Delta = 0$,

$$\left. \frac{S_1}{S_2} \right|_{t_\Delta=0} = U_\Delta(0; \rho), \quad (\text{B4})$$

thus the ratio only depends on the parameter Δ , and the curves for different system sizes L are expected to collapse together. To be specific, we plot the ratio of $\langle S_1 \rangle / \langle S_2 \rangle$ as the function of the target overlapping area Δ for different system size L in Fig. 8(a). It is clear that the critical point is $\Delta_c \approx 0.0945$, since different curves cross at this point, where the density of disks is $\rho = 2$. After rescaling Δ to $L^{1/\nu'} t_\Delta$, the curves coincide when $\nu' = 4/3$, as shown in Fig. 8(b), thus the scaling exponent ν' is the same as ν .

The critical exponent ν can also be estimated more accurately from the position of the peak in $S_2(L)$, where the reduced control parameter t_Δ^{peak} of the peak position has a scaling form, $t_\Delta^{\text{peak}} \propto L^{-1/\nu}$, in Fig. 9(a) the slope of the dashed line is $-1/\nu = -0.7506$. Figure 9(b) shows the size of the largest cluster $\langle S_1 \rangle$ and the second largest cluster $\langle S_2 \rangle$ at Δ_c for different system sizes, with the same results as in Fig. 3(b), and the slopes derived from the fitted lines correspond to the fractal dimensions, $d_f = 1.886(8)$. According to Eq. (7), the ratio of the critical exponents β/ν and γ/ν can be obtained when Δ is the control parameter, which corresponds to the slopes -0.1083 and 1.815 in Figs. 9(c) and 9(d) respectively. These critical behaviors of the setting Δ as control parameter are identical with the behaviors of those of varying ρ .

- [1] M. B. Isichenko, Percolation, statistical topography, and transport in random media, *Rev. Mod. Phys.* **64**, 961 (1992).
- [2] A. A. Saberi, Recent advances in percolation theory and its applications, *Phys. Rep.* **578**, 1 (2015).
- [3] M. Li, R.-R. Liu, L. Lü, M.-B. Hu, S. Xu, and Y.-C. Zhang, Percolation on complex networks: Theory and application, *Phys. Rep.* **907**, 1 (2021).
- [4] S. R. Broadbent and J. M. Hammersley, Percolation processes: I. Crystals and mazes, *Math. Proc. Camb. Philos. Soc.* **53**, 629 (1957).
- [5] G. Ódor, Universality classes in nonequilibrium lattice systems, *Rev. Mod. Phys.* **76**, 663 (2004).
- [6] J.-Q. Dong, Z. Shen, Y. Zhang, Z.-G. Huang, L. Huang, and X. Chen, Finite-size scaling of clique percolation on two-dimensional Moore lattices, *Phys. Rev. E* **97**, 052133 (2018).
- [7] K. Christensen and N. Moloney, *Complexity and Criticality*, Imperial College Press Advanced Physics Texts (World Scientific, Singapore, 2005).
- [8] N. Araújo, P. Grassberger, B. Kahng, K. J. Schrenk, and R. M. Ziff, Recent advances and open challenges in percolation, *Eur. Phys. J.: Spec. Top.* **223**, 2307 (2014).
- [9] B. Vigolo, C. Coulon, M. Maugey, C. Zakri, and P. Poulin, An experimental approach to the percolation of sticky nanotubes, *Science* **309**, 920 (2005).
- [10] C. Grimaldi and I. Balberg, Tunneling and nonuniversality in continuum percolation systems, *Phys. Rev. Lett.* **96**, 066602 (2006).
- [11] A. Álvarez-Álvarez, I. Balberg, and J. P. Fernández-Álvarez, Invariant percolation properties in some continuum systems, *Phys. Rev. B* **104**, 184205 (2021).
- [12] S. H. Park, J. Y. Hwang, G. S. Park, J. H. Ha, M. S. Zhang, D. Kim, D. J. Yun, S. Lee, and S. H. Lee, Modeling the electrical resistivity of polymer composites with segregated structures, *Nat. Commun.* **10**, 2537 (2019).
- [13] P. Gniewek and O. Hallatschek, Fluid flow through packings of elastic shells, *Phys. Rev. E* **99**, 023103 (2019).
- [14] J. Mendez, P. K. Annamalai, S. J. Eichhorn, R. Rusli, S. J. Rowan, E. J. Foster, and C. Weder, Bioinspired mechanically adaptive polymer nanocomposites with water-activated shape-memory effect, *Macromolecules* **44**, 6827 (2011).
- [15] Y. Chen and C. A. Schuh, Elasticity of random multiphase materials: Percolation of the stiffness tensor, *J. Stat. Phys.* **162**, 232 (2016).
- [16] I. Glauche, W. Krause, R. Sollacher, and M. Greiner, Continuum percolation of wireless *ad hoc* communication networks, *Physica A* **325**, 577 (2003).
- [17] H. Döring, G. Faraud, and W. König, Connection times in large *ad-hoc* mobile networks, *Bernoulli* **22**, 2143 (2016).
- [18] I. Breskin, J. Soriano, E. Moses, and T. Tlusty, Percolation in living neural networks, *Phys. Rev. Lett.* **97**, 188102 (2006).
- [19] J. Soriano, M. R. Martínez, T. Tlusty, and E. Moses, Development of input connections in neural cultures, *Proc. Natl. Acad. Sci. USA* **105**, 13758 (2008).
- [20] S. Mertens and C. Moore, Continuum percolation thresholds in two dimensions, *Phys. Rev. E* **86**, 061109 (2012).
- [21] J. Li and M. Östling, Percolation thresholds of two-dimensional continuum systems of rectangles, *Phys. Rev. E* **88**, 012101 (2013).
- [22] J. A. Quintanilla and R. M. Ziff, Asymmetry in the percolation thresholds of fully penetrable disks with two different radii, *Phys. Rev. E* **76**, 051115 (2007).
- [23] J.-T. Li and S.-L. Zhang, Finite-size scaling in stick percolation, *Phys. Rev. E* **80**, 040104(R) (2009).
- [24] Y. Y. Tarasevich and A. V. Eserkepov, Percolation of sticks: Effect of stick alignment and length dispersity, *Phys. Rev. E* **98**, 062142 (2018).
- [25] V. Sasidevan, Continuum percolation of overlapping disks with a distribution of radii having a power-law tail, *Phys. Rev. E* **88**, 022140 (2013).
- [26] E. T. Gawłinski and H. E. Stanley, Continuum percolation in two dimensions: Monte Carlo tests of scaling and universality for non-interacting discs, *J. Phys. A: Math. Gen.* **14**, L291 (1981).
- [27] T. Vicsek and J. Kertesz, Monte Carlo renormalisation-group approach to percolation on a continuum: test of universality, *J. Phys. A: Math. Gen.* **14**, L31 (1981).
- [28] A. Geiger and H. E. Stanley, Tests of universality of percolation exponents for a three-dimensional continuum system of interacting waterlike particles, *Phys. Rev. Lett.* **49**, 1895 (1982).
- [29] B. Skyrms and R. Pemantle, A dynamic model of social network formation, *Proc. Natl. Acad. Sci. USA* **97**, 9340 (2000).
- [30] J. M. Pacheco, A. Traulsen, and M. A. Nowak, Coevolution of strategy and structure in complex networks with dynamical linking, *Phys. Rev. Lett.* **97**, 258103 (2006).
- [31] S. Poledna and S. Thurner, Elimination of systemic risk in financial networks by means of a systemic risk transaction tax, *Quant. Financ.* **16**, 1599 (2016).
- [32] A. Scirè, I. Tuval, and V. M. Eguíluz, Dynamic modeling of the electric transportation network, *Europhys. Lett.* **71**, 318 (2005).
- [33] R.-R. Liu, C.-X. Jia, and Y.-C. Lai, Remote control of cascading dynamics on complex multilayer networks, *New J. Phys.* **21**, 045002 (2019).
- [34] F. D. Iudin, D. I. Iudin, and V. B. Kazantsev, Percolation transition in active neural networks with adaptive geometry, *JETP Lett.* **101**, 271 (2015).
- [35] I. Y. Tyukin, D. Iudin, F. Iudin, T. Tyukina, V. Kazantsev, I. Mukhina, and A. N. Gorban, Simple model of complex dynamics of activity patterns in developing networks of neuronal cultures, *PLoS ONE* **14**, e0218304 (2019).
- [36] F. Y. Kalle Kossio, S. Goedeke, B. van den Akker, B. Ibarz, and R.-M. Memmesheimer, Growing critical: Self-organized criticality in a developing neural system, *Phys. Rev. Lett.* **121**, 058301 (2018).
- [37] N. Tsakiris, M. Maragakis, K. Kosmidis, and P. Argyrakis, Percolation of randomly distributed growing clusters: Finite-size scaling and critical exponents for the square lattice, *Phys. Rev. E* **82**, 041108 (2010).
- [38] N. Tsakiris, M. Maragakis, K. Kosmidis, and P. Argyrakis, Percolation of randomly distributed growing clusters: The low initial density regime, *Eur. Phys. J. B* **81**, 303 (2011).
- [39] O. Melchert, Universality class of the two-dimensional randomly distributed growing-cluster percolation model, *Phys. Rev. E* **87**, 022115 (2013).
- [40] A. Coniglio, H. E. Stanley, and W. Klein, Site-bond correlated-percolation problem: A statistical mechanical model of polymer gelation, *Phys. Rev. Lett.* **42**, 518 (1979).

- [41] Z. Gao and Z. Yang, The percolating properties of dissociated monomers in a dimer adsorption process, *Physica A* **255**, 242 (1998).
- [42] Y. Y. Tarasevich and S. C. van der Marck, An investigation of site-bond percolation on many lattices, *Int. J. Mod. Phys. C* **10**, 1193 (1999).
- [43] M. Dolz, F. Nieto, and A. J. Ramirez-Pastor, Dimer site-bond percolation on a square lattice, *Eur. Phys. J. B* **43**, 363 (2005).
- [44] M. Dolz, F. Nieto, and A. J. Ramirez-Pastor, Site-bond percolation of polyatomic species, *Phys. Rev. E* **72**, 066129 (2005).
- [45] M. I. González-Flores, A. A. Torres, W. Lebrecht, and A. J. Ramirez-Pastor, Site-bond percolation in two-dimensional kagome lattices: Analytical approach and numerical simulations, *Phys. Rev. E* **104**, 014130 (2021).
- [46] M. X. Liu, J. F. Fan, L. S. Li, and X. S. Chen, Continuous percolation phase transitions of two-dimensional lattice networks under a generalized Achlioptas process, *Eur. Phys. J. B* **85**, 132 (2012).
- [47] R. M. Ziff, Correction-to-scaling exponent for two-dimensional percolation, *Phys. Rev. E* **83**, 020107(R) (2011).
- [48] M. E. J. Newman and R. M. Ziff, Efficient Monte Carlo algorithm and high-precision results for percolation, *Phys. Rev. Lett.* **85**, 4104 (2000).
- [49] D. ben Avraham and S. Havlin, *Diffusion and Reactions in Fractals and Disordered Systems* (Cambridge University Press, Cambridge, 2005).
- [50] M. F. Sykes and J. W. Essam, Exact critical percolation probabilities for site and bond problems in two dimensions, *J. Math. Phys.* **5**, 1117 (1964).
- [51] B. Nienhuis, Exact critical point and critical exponents of $O(n)$ models in two dimensions, *Phys. Rev. Lett.* **49**, 1062 (1982).
- [52] A. Margolina, H. Herrmann, and D. Stauffer, Size of largest and second largest cluster in random percolation, *Phys. Lett. A* **93**, 73 (1982).